

An image processing approach for converging ASTER-derived spectral maps for mapping Kolhan limestone, Jharkhand, India

Arindam Guha^{1,*}, K. Vinod Kumar¹, E. N. Dhananjaya Rao² and Reshma Parveen³

¹National Remote Sensing Centre, Balanagar, Hyderabad 500 625, India

²Andhra University, Visakhapatnam 530 003, India

³Jharkhand Space Application Centre, Ranchi 834 004, India

In the present study, we have attempted the delineation of limestone using different spectral mapping algorithms in ASTER data. Each spectral mapping algorithm derives limestone exposure map independently. Although these spectral maps are broadly similar to each other, they are also different at places in terms of spatial disposition of limestone pixels. Therefore, an attempt is made to integrate the results of these spectral maps to derive an integrated map using minimum noise fraction (MNF) method. The first MNF image is the result of two cascaded principal component methods suitable for preserving complementary information derived from each spectral map. While implementing MNF, noise or non-coherent pixels occurring within a homogeneous patch of limestone are removed first using shift difference method, before attempting principal component analysis on input spectral maps for deriving composite spectral map of limestone exposures. The limestone exposure map is further validated based on spectral data and ancillary geological data.

Keywords: Limestone, minimum noise fraction, spectral mapping, image processing.

ADVANCED Space Borne Thermal Emission and Reflection Radiometer (ASTER) data have already shown their potential for mineral exploration, specially for delineating different alteration zones and associated lithology¹⁻⁶. ASTER has the capability of mapping different rocks and minerals. ASTER data can be used for deriving different indices for delineating carbonate minerals⁷⁻¹⁰. Therefore, these data have also been successfully used for delineating limestone^{11,12}. In these studies, efforts were focused to demarcate the limestone based on spectral signatures of pure calcite mineral as the end member. But it is always essential to analyse the spectral features of the target to be spatially mapped for understanding its diagnostic absorption signature. Once the diagnostic absorption signature of the target is characterized in the laboratory, it is

essential to compare the image spectra of the target with its laboratory counterpart to analyse the consistency of diagnostic absorption feature of end members from the exposure to the pixel of the satellite image.

Moreover, as the exposure size of the target changes, the spectral response of the pixel containing the target would also vary. Therefore, we need to use different spectral mapping algorithms to map a target which has surface exposures of variable sizes under the tropical set-up. Further, it is also essential to converge the results of the different spectral maps of the same target to derive a composite exposure map. This convergence would allow to preserve the commonalities of the input spectral maps. Therefore, the aim of the present study was to derive different ASTER-based spectral maps for limestone and converge the results of different spectral maps to derive a composite limestone map of the study area.

Integration of the results of different spectral maps to derive a composite map is essential for a target like limestone which is known for limited exposures under tropical weathering set-up. The composite limestone exposure map thus derived can be used as an input for detailed petrographic and mineralogical study for narrowing down the limestone pockets suitable for mining. In order to map limestone based on spectral features, an attempt is also made to analyse the diagnostic spectral feature of limestone in the laboratory and in the ASTER image to spectrally characterize limestone having its broad spectral feature recorded in the ASTER bandwidth. Spectral features of carbonate minerals are well studied and this understanding helps in identifying the diagnostic spectral signature of limestone^{12,13}.

The study area is located in the eastern part of India in the state of Jharkhand (Figure 1). Jharkhand is known for bauxite, iron, coal, limestone, mica, uranium and base metal reserves of the country. Field work was carried out for collecting the rock samples for spectroscopic studies and also for updating the existing geological map based on field information and image interpretation of ASTER false colour composites (FCC). Field work is also essential to have an overall understanding of the geological

*For correspondence. (e-mail: arindam_g@nrsc.gov.in)

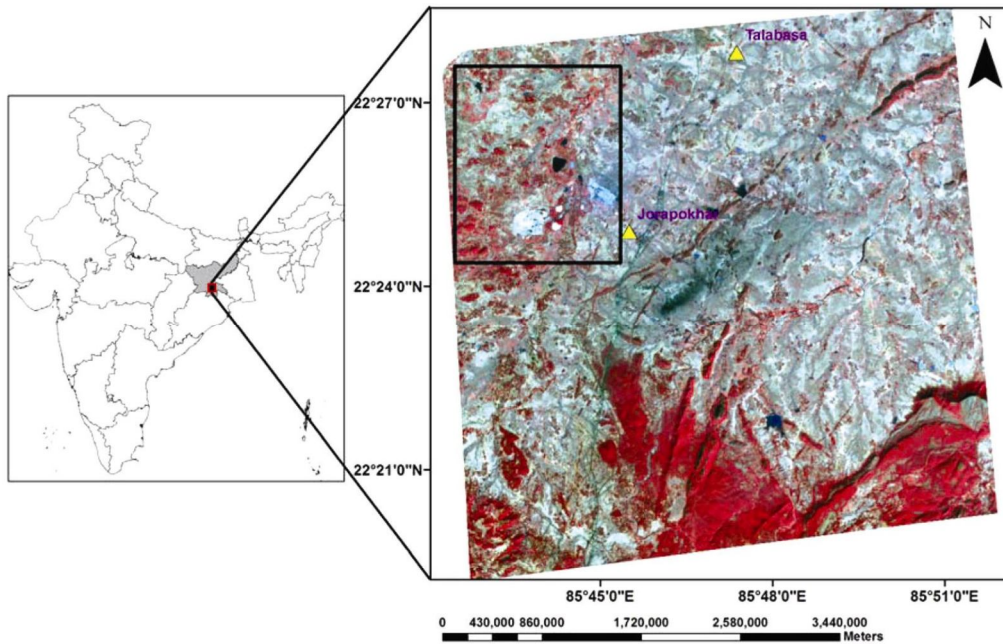


Figure 1. Study area shown by a rectangle in the ASTER false colour composite image derived using red–green–blue colour space (red is the third band, green the second band and blue the first band of ASTER image).

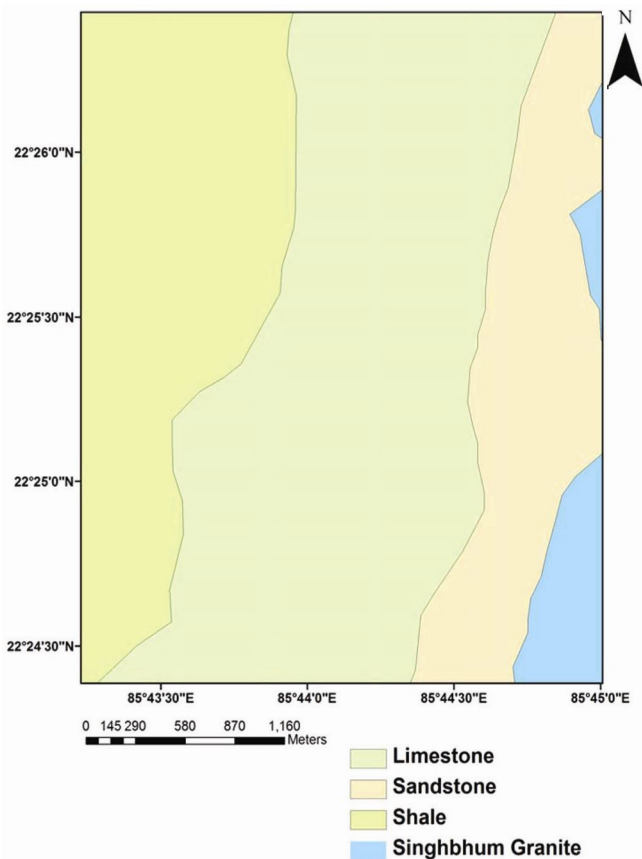


Figure 2. Modified (based on interpretation of ASTER false-colour composite image supplemented with field survey along selected traverses) geological map of the study area (original source map: Geological Survey of India; GSI M&C Division ER/Kolkata, D.O. No. 10/2006). Geological boundaries of limestone–shale and limestone–sandstone are modified based on field exposures of limestone occurrences.

setting and specially the knowledge of limestone occurrences in the study area.

Limestone of the area belongs to the proterozoic Kolhan Group. The Kolhan Group of rocks unconformably overlie the granite-gneiss and are restricted to the north-eastern, eastern and southeastern portion of the study area (Figures 1 and 2). The Group consists of purple sandstone and conglomerate at the base, followed upward successively by thick sequences of argillite, stromatolitic limestone and shale/phyllite¹⁴. The general strike of the Kolhan Group of rocks is along NNE–SSW (Figure 2). In general, the entire sequence of the Kolhan Group is a fining upward sequence. The vertical and lateral facies variation in Kolhan is due to the superimposition of retrograding shorelines on an earlier prograding alluvial fan (sand complex) laid down in the embayment¹⁵. The Kolhan Group of rocks occurring on the Singhbhum craton can be lithologically correlated with the late Meso–Neoproterozoic successions from other cratonic blocks of peninsular India¹⁶. Therefore mapping of the limestone and carbonate-rich facies within this particular sedimentary succession using spectral features of limestone would be significant. The spectral mapping approach of limestone delineation may also be extended to similar basins of other cratonic blocks in India and abroad¹⁶. Moreover, the study area is already well known for limestone mines, which provide the raw materials for cement industries¹⁷. At present, a few mines are operative in the area¹⁷; but, it is essential to extend the mine reserves to cater to the future requirement of the mining industry. Therefore, the present study aims to map limestone exposures by processing ASTER data using spectral feature of limestone as the key.

Table 1. Specification of ASTER VNIR–SWIR bands (date of scene: 23 March 2006)

Satellite data	Data product	Spectral bands	Spectral range (µm)	Spatial resolution (m)	Radiometric resolution
ASTER data	VNIR	1	0.5–0.60	15	8
		2	0.63–0.69	15	8
		3N	0.78–0.86	15	8
		3B	0.78–0.86	15	8
	SWIR	4	1.60–1.70	30	8
		5	2.145–2.185	30	8
		6	2.185–2.225	30	8
		7	2.235–2.285	30	8
		8	2.295–2.365	30	8
		9	2.360–2.430	30	8

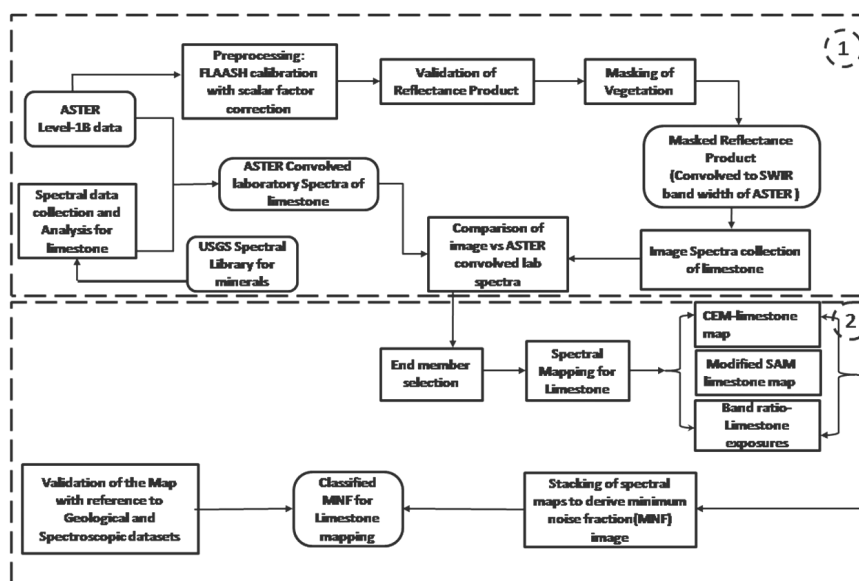


Figure 3. Flowchart of methodology. Two blocks are shown with a dashed outline. See text for more details.

Materials and methodology

ASTER Level-1B data (only visible-near infrared (VNIR)–shortwave infrared (SWIR) bands) are used in the present study. Detailed specification of ASTER VNIR–SWIR bands is provided in Table 1. ASTER SWIR bands are used for delineating limestone. The VNIR bands are used during pre-processing steps for masking the vegetation cover in the image and for validating relative reflectance image. The geological map prepared by the Geological Survey of India (Figure 2) is also used for validation of the results.

ASTER Level-1B VNIR–SWIR datasets (‘at-sensor’ radiance data with geometric correction applied to the data) are used in the present study as these bands are sufficient to delineate limestone from the associated soil and forested background based on their diagnostic spectral signature within the VNIR–SWIR domain. Specially SWIR bands of ASTER channels are known for their potential for delineating mineralogy and different rock types and also suitability for spatial mapping⁷. The data

are converted to scaled reflectance before using the same for mapping the limestone based on the ‘spectral signature’. A flow chart (Figure 3) is furnished for summarizing the methodology. Preprocessing steps are grouped under block-1 and processing steps under block-2 of the flow chart.

Spectral profile collection of rock samples

Spectral profiles are collected using Fieldspec3© spectroradiometer (manufactured by Analytical System Device Inc.) under controlled laboratory environment. The spectroradiometer is operative in the wavelength domain of 350–2500 nm. It has good signal-to-noise ratio with finer spectral resolution (3 nm @ 700 nm and 10 nm @ 1400/2100 nm) and finer spectral sampling interval (1.4 nm @ 350–1050 nm; 2 nm @ 1000–2500 nm)¹⁸. Spectral resolution is fine enough to detect the subtle absorption features characteristic of the constituent minerals of the rock. Fieldspec3© spectroradiometer has two types of detectors: a 512 element Si photodiode detector operative

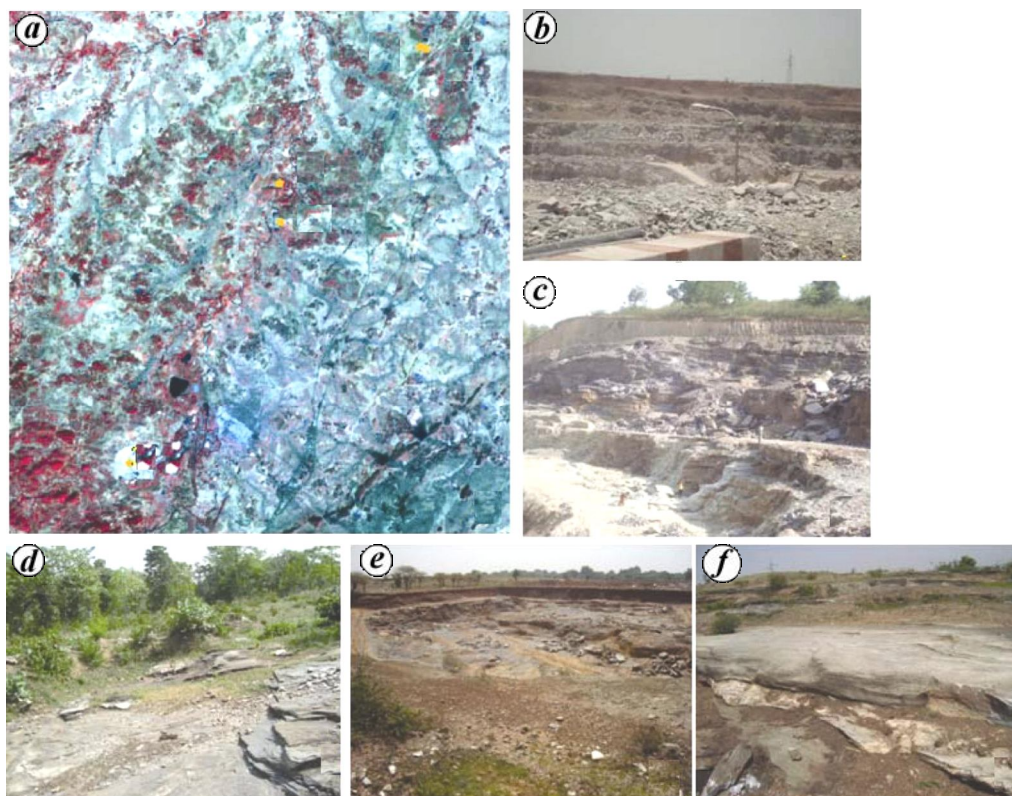


Figure 4. Limestone exposures in the study area. *a*, Location of each exposure is plotted in VNIR FCC. *b–f*, Field photographs of mines. *b*, Jhinkpani Mines; *c*, Surjabhasa Mines; *d*, Indikuri Limestone; *e*, Singh Pokharia limestone; *f*, Surface exposures near Singh Pokharia.

Table 2. Description of few major exposures

Sample no.	Field description	Latitude	Longitude	Place
1	Thick bedded deposits	22°25'01.97"N	85°43'48.58"E	Surface exposures of Jhinkpani Mines
2	Pocket deposits, small in size, weathered	22°27'55.98"N	85°45'49.79"E	Surface exposures of Surjabhasa Mines
3	Pocket deposits within shale, small exposures, weathered	22°28'24.16"N	85°45'41.81"E	Surface exposures of Indikuri Limestone
4	Bedded deposits, small exposures, weathered	22°30'03.42"N	85°47'43.08"E	Surface exposures of Singh Pokharia limestone
5	Bedded deposits, small exposures, weathered	22°30'04.72"N	85°47'38.80"E	Surface exposures near Singh Pokharia

in 350–1000 nm range and two separate InGaAs photodiodes operative in 1000–2500 nm range. The methodology adopted for collecting the rock spectra and post-processing has already been discussed in the literature^{19,20}.

The samples are collected from the exposures of varied sizes and modes of occurrence (Figure 4). Details of the exposures with their geo-locations are given in Table 2. For each exposure, 3–4 samples are collected for spectroscopic studies. Rock samples are cut into 4" × 5" to 5" × 7" rectangular pieces. The sample size range used is well within the size norms of the samples analysed at the Jet Propulsion Laboratory associated with National Aeronautics and Space Administration, USA²¹.

Reflectance profiles of the rock samples are collected by vertically pointing the measurement gun which contains the fibre optics. The light source (halogen lamp) illuminates the sample with an angle (with respect to imaginary vertical drawn above the sample) and the spectral profiles are collected by keeping the bare fibre optics of the spectroradiometer vertically over the sample. This makes the phase angle 45° (phase angle corresponds to the angle between the illumination source and measurement points)^{19,20}. The reflected energy of the rock samples thus collected is due to the volume scattering of the rock. The energy reflected by volume scattering represents internal chemical (mineralogical) characters as well. The

field-of-view of fore optics, used for reflectance measurement is 25° .

Twenty spot observations per sample are recorded and averaged to get the characteristic spectral curve for each limestone specimen. Further, spectral profiles of two or three sample spots are measured for each limestone sample to record the 'representative' spectra based on averaging of the spectral profiles of each spot. Averaging of multiple measurements has an added advantage in suppressing insignificant kinks in the spectral profiles of the rock. Limestone laboratory spectra of each of the significant exposures are illustrated in Figure 5a. Limestone spectra are re-sampled to ASTER wavelength to derive ASTER convolved laboratory spectra for limestone for each significant known exposure (Figure 5b). Based on the inspection of laboratory derived limestone spectra and ASTER convolved counterparts, it is understood that limestone has diagnostic absorption feature at around 2335 nm in laboratory spectra, which has been convolved to 2330 nm or 2.33 μm in ASTER convolved counterpart of laboratory spectra.

ASTER data pre-processing

ASTER Level 1B data are corrected for reflectance using FLAASH© (Fast Line of Sight Spectral Analysis of

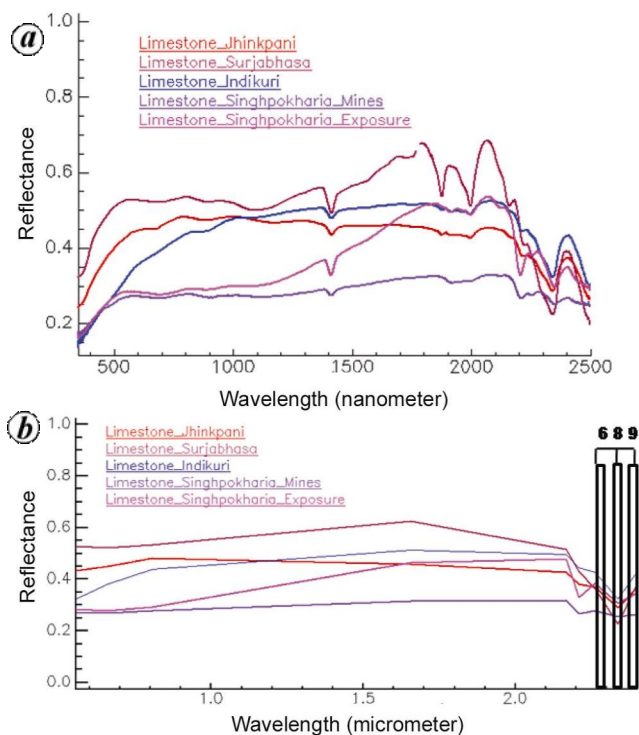


Figure 5. a, Laboratory spectra of limestone samples collected from field locations depicted in Figure 2. b, ASTER convolved laboratory spectra of limestone samples. Relative positions of bands 6, 8, 9 are illustrated over ASTER convolved image spectra.

Spectral Hypercube) algorithm. This is a physics-based atmospheric correction algorithm suitable for atmospheric correction in VNIR and SWIR domains. FLAASH© is developed based on MODTRAN4© (Moderate Resolution Atmospheric Transmission) calculations (physical model to characterize the atmosphere) that use the solar angles, the mean surface elevation, etc. for calibration. The algorithm operates on the assumption of certain calibration models using atmospheric, aerosol type and visibility range^{22,23}. Parameters such as the time of data acquisition, centre of the scene and average altitude information are also provided in the FLAASH© interface to calibrate the ASTER radiance image to scaled reflectance image. Once the data are calibrated using FLAASH©, the mean image spectra of the terrain elements (deciduous forest cover and limestone) collected from few regions are compared with the ASTER convolved laboratory spectra of the respective terrain elements. Initially, it has been found that these spectra do not perfectly match with other. Therefore, a scalar factor is used to further scale the FLAASH© calibrated ASTER data. The scalar factor for each band is derived from the division of the image spectra of deciduous forest by the laboratory spectra of the same terrain element. The two-step atmospheric correction method described above (FLAASH© calibration followed by scaling using a factor for each band) is often used to minimize the instrument noise, solar irradiance uncertainty and also the atmospheric variability resulting due to topographic variation²⁴. Once the apparent reflectance image is derived (Figure 6a), spectral profiles of deciduous tree and limestone derived from the image are compared with the ASTER convolved (VNIR–SWIR) spectral profiles of the same elements collected in the laboratory (Figure 6b and c). Limestone laboratory spectra are collected from spectral database of limestone derived from the present study and the representative vegetation laboratory spectra of deciduous tree is taken from the catalogue of laboratory spectra of the United States Geological Survey (USGS). It has been observed that the ASTER image spectra of the aforesaid terrain elements match well with the ASTER convolved laboratory spectra counterparts, specially for the absorption features (Figure 6b and c). This justifies the accuracy of the relative reflectance image to be used for spectral mapping.

ASTER data processing

After reflection calibration, Normalized Difference Vegetation Index (NDVI) is calculated for masking the most dominant surface elements (forest cover) from the scaled reflectance image. Due to limited spectral dimensionality, terrain elements having closely spaced absorption features would be spectrally similar in ASTER data. Therefore, few end members can only be delineated in ASTER data based on spectral features. Vegetation masking was

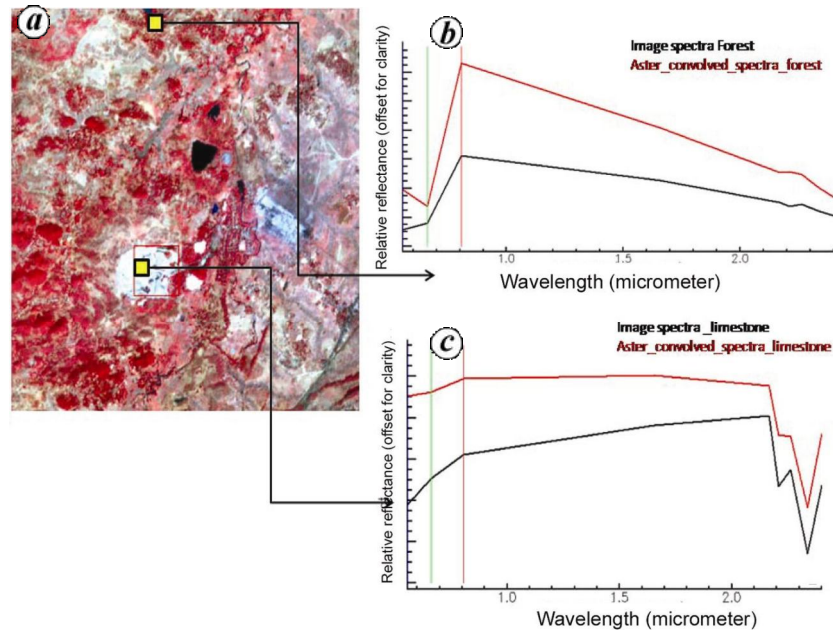


Figure 6. *a*, Calibrated (apparent reflectance) ASTER data (FCC of red–green–blue colour space (band 3, 2 and 1 respectively) as defined in Figure 1). *b*, Image spectra of deciduous forest plotted with the ASTER convolved deciduous forest spectra to show the quality of reflectance product. *c*, SWIR band image spectra of limestone plotted with representative ASTER convolved laboratory spectra.

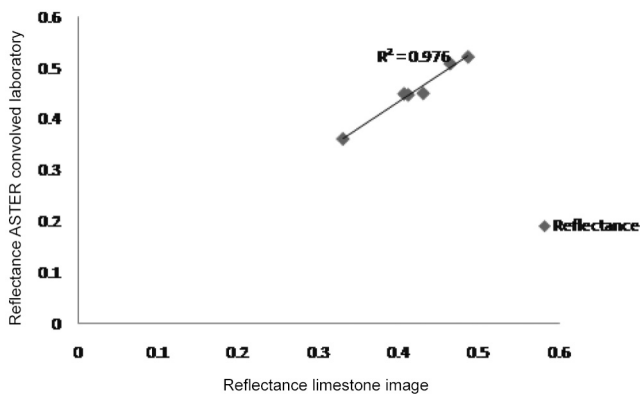


Figure 7. Comparison between image spectra of limestone and ASTER SWIR convolved laboratory spectra of limestone.

essential to segregate out ‘uncovered’ pixels of the study area for spectral mapping. In the present study, ASTER channel 2 (red band) and channel 3 (NIR) are used for suppressing the vegetation. Masking is carried out based on the NDVI value of vegetation derived from the above-mentioned ASTER channels. The masking rule (i.e. range of NDVI values required to be specified to suppress the vegetation) is selected iteratively for ensuring complete suppressing of forest or vegetation cover.

While analysing the ASTER convolved limestone spectra, it is found that the characteristic absorption signature for limestone occurs at the SWIR domain (Figure 5 *b*). Therefore, ASTER convolved laboratory spectra of limestone are further re-sampled to the bandwidth of the ASTER SWIR channels. These laboratory spectral pro-

files of limestone are then continuum-removed and compared with the continuum-removed mean image spectra of limestone, collected from the pixels representing open-cast mines. Continuum removal method is a reflectance normalization method applied to both the reference spectra and the image for enhancing and separating the specific absorption features of interest (i.e. for limestone). The high degree of correlation between the continuum-removed image spectra and the continuum-removed laboratory-spectra (ASTER convolved) of limestone indicates the capability of ASTER data in preserving the diagnostic spectral feature of limestone (Figure 7). Hence the image spectra of limestone collected from SWIR bands of open-cast mine have been taken as an end member for spectral mapping of ASTER SWIR image based on the spectral angle mapper and relative band depth mapping methods. It is important to note that the selection of the image spectra of the pixels of the limestone outcrops as end members also ensures that the spectral end member suitably represents well the spectral characteristics of the surface of outcrop of limestone by incorporating possible variations resulted from surface weathering and association. The potential advantage and utility of image spectra as end member for spectral mapping has been discussed in the literature^{25–27}. However, laboratory spectra (after convolving to the ASTER SWIR band) is utilized in sub-pixel for spectral mapping algorithm known as constrained energy minimization method as these spectra are generally used for decomposing image spectra to their sub-components (i.e. target spectra and background spectra) in sub-pixel mapping²⁸.

Results

As mentioned earlier, we have few selected spectral mapping algorithms for processing ASTER data to delineate limestone exposures of the study area. In this regard, both per-pixel and sub-pixel mapping algorithms have been used to delineate limestone exposures of varying sizes. In this regard, we have used ASTER SWIR image as input and ASTER SWIR image spectra of limestone as end member for deriving limestone distribution map using spectral angle mapper (SAM) and relative band width (RBD) algorithms. Limestone SWIR bands actually preserve diagnostic absorption feature of limestone, as is evident from Figure 6 *c*.

As mentioned earlier, mapping algorithms used for limestone mapping are broadly subdivided into two segments: per-pixel mapping and sub-pixel mapping methods. Per-pixel methods are used to derive the limestone map based on the assumption that the spectra of limestone pixel delineated by these algorithms would be similar to image spectra of limestone mines. This would be the case for all the limestone exposures which are large in size. Two per-pixel mapping methods are used in the present study. These are SAM and RBD methods. SAM is an effective mapping technique suitable for per-pixel detection of targets. It is used to spatially map a target based on the derivation of solid angle subtended between pixel spectra and reference end member spectra in the n -dimensional data space of the ASTER image (where n is the number of bands of the image subjected to SAM classification)^{29,30}. The SAM rule image thus derived for limestone is a grey-scale image, in which pixels with darker tone are the spectral representatives of the desired target, i.e. limestone. Further, SAM map is multiplied by -1 to illustrate limestone pixels with brighter tone, which has been further density sliced with red colour (Figure 8 *a*). Red colour in this map is indicative of the spectra of the pixels having 'lowest spectral angle' with respect to input image spectra. In addition to above, the absorption minima (i.e. band with lowest reflection value) and its associated shoulders (i.e. bands with highest reflectance on either side of the absorption band) imprinted in the reflectance profile of limestone pixel have been considered as the criteria for deriving RBD ratio image. The band ratio, which is derived based on bands at the absorption depth and also at the shoulder of an absorption feature helps in understanding the depth of absorption^{9,26}. Therefore, the ratio is regarded as band depth (BD) image. In this regard, we have chosen 6, 8 and 9 bands of ASTER VNIR-SWIR image (i.e. 3, 5 and 6 SWIR bands; Figure 5 *b*). This RBD image is similar to the three-point ratio image as proposed by earlier workers²⁷. However, they used bands 7, 8 and 9 of ASTER data for delineating carbonate mineral. The band ratio image is also colour-graded with red colour to indicate limestone pixels characterizing the highest absorption depth in this band (Figure 8 *c*)^{9,26}.

There are exposures which have spatial size smaller than the size of ASTER SWIR pixels. In such cases, spectra of limestone-bearing pixels (modified due to spectral mixing) would be subdued in comparison to the pixels occupied entirely by limestone. The spectra of these pixels have been decomposed based on the input reference ASTER convolved laboratory spectra in two segments; one is the target and the other is background based on the implementation of CEM method. In this method, the spectral character of background is mathematically derived from the covariance matrix of ASTER data based on the diagnostic spectral profile of the target. CEM method is suitable for mapping a target which has a wide distribution, as is the case in the present study area³¹. CEM method is effective, provided background and foreground are linearly mixed^{25,31}.

Different spectral maps derived using the aforesaid methods could delineate limestone pixels with similar spatial distribution although have subtle variations (Figure 8 *a-c*). The spatial distribution of limestone pixels varies from place to place in these maps. For example, colour-shaded SAM, CEM and RBD images have slightly different distribution of limestone on the edge of the limestone quarry. This has been illustrated in the zoomed part of colour-shaded spectral maps; where limestone pixels are demarcated with red colour (Figure 8 *a-c*).

However, it is always preferable to derive a conclusive map for targeting economic rocks like limestone by bringing together complementary information from each spectral map. Therefore two-cascaded principal component method, known as a minimum noise fraction (MNF) method, is used to integrate these spectral maps to derive a composite map. In general, MNF image is used to bring together the complementary information of different spectral maps by removing noise and reducing dimensionality in hyperspectral data. MNF is used to order spectral bands according to the information content based on the assumption that noise is non-correlative in each input band^{6,32,33}. MNF is a suitable approach to condense most of the important spectral information in one or few bands. Further, MNF images have also been used to detect targets, specially different alteration minerals associated with hydrothermal deposits^{34,35}. Here, we have used MNF to converge the result of different spectral mapping algorithms used to delineate limestone. In each spectral map, noises are represented either by non-coherent pixels occurring within continuous limestone patch or randomly distributed at the edge of homogeneous patches of limestone exposures. A non-coherent distributions of pixels are evident at the edge of the big limestone quarry (zoomed part of Figure 8 *a-c*). These pixels are eliminated at the first stage of MNF computation based on shift difference method. For calculating noise, shift difference method is performed on the pixel clusters (specified by the user) by calculating the differences in the value of each pixel from the adjacent one occurring below or to the right of

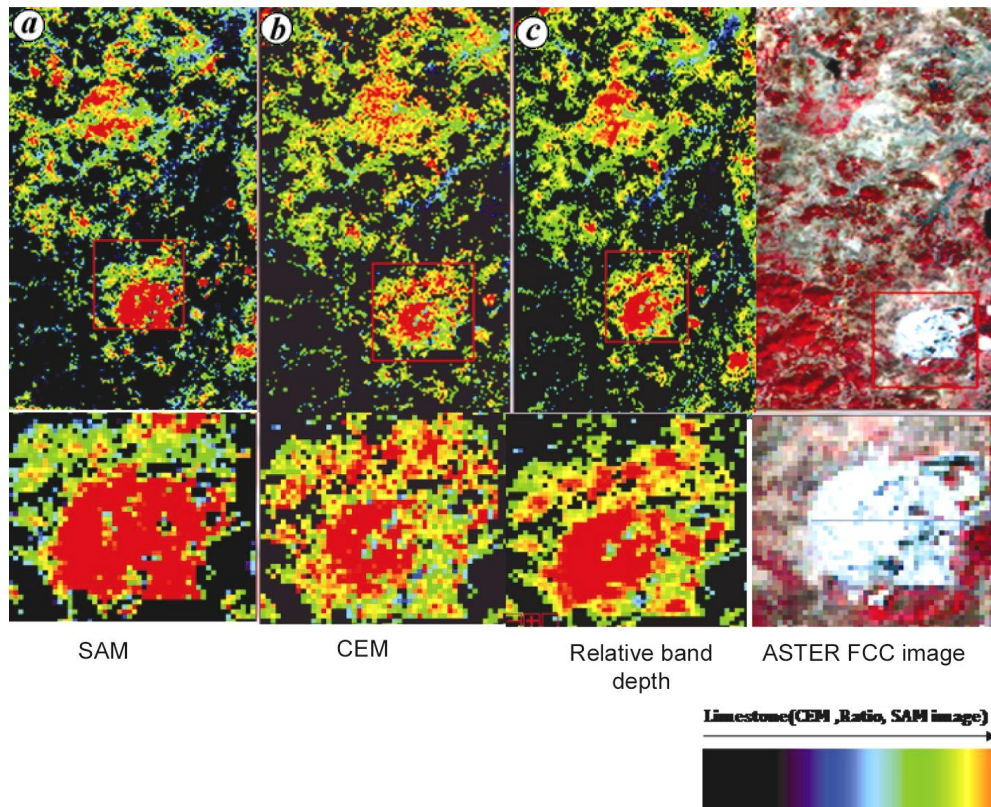


Figure 8. Inverted spectral angle mapper (SAM) (*a*), constrained energy minimization (CEM) (*b*) image and relative band depth (RBD) image (band 6 + band 9)/2*band 7 (*c*). ASTER FCC image showing limestone open cast is also provided for visual comparison. Carbonate-rich zones are graded with red colour (as parameters like low SAM angle, high CEM value and high RBD values are illustrated with red colour in SAM, CEM, RBD map respectively for indicating limestone). (Inset *a-c*, Colour graded open cast of limestone).

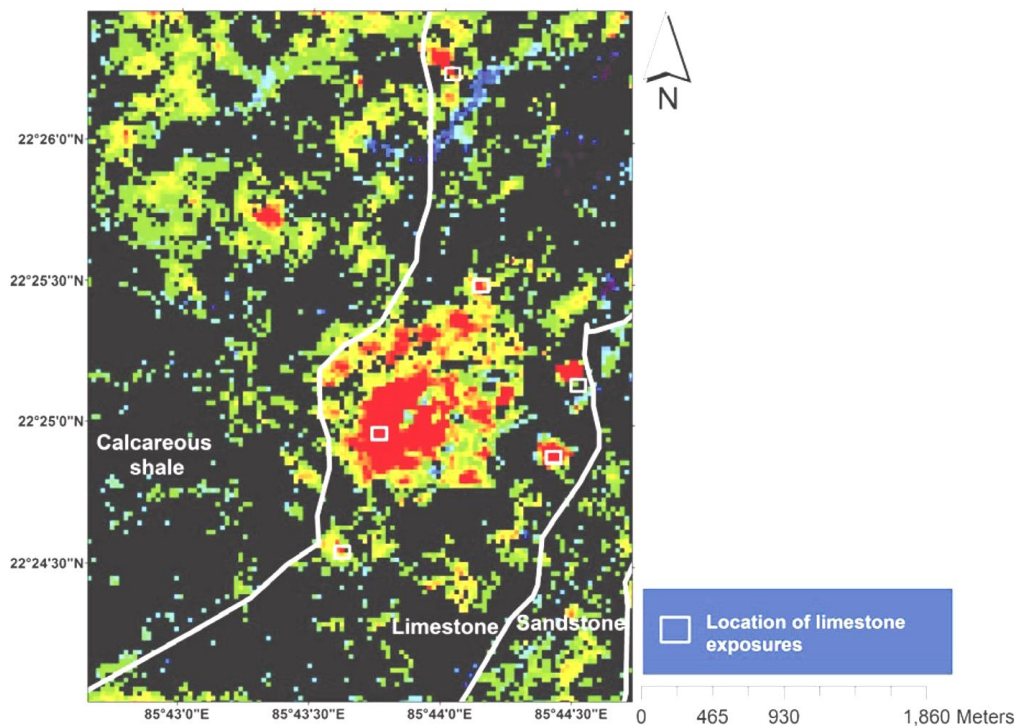


Figure 9. Limestone map showing carbonate-rich pockets (red in colour) plotted with the geological boundary of limestone-shale (calcareous) and limestone-sandstone.

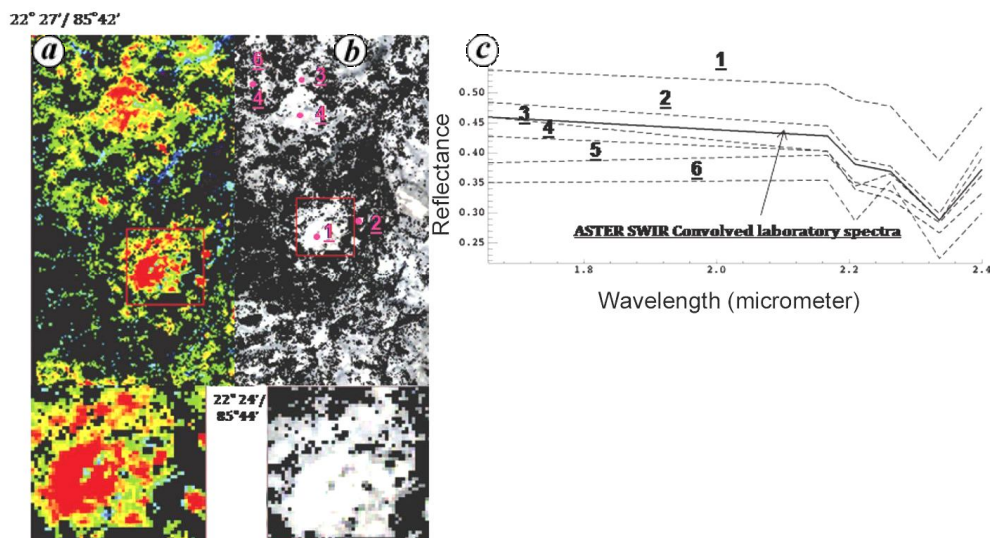


Figure 10. *a*, MNF-1 image derived from three spectral maps (SAM, CEM, RBD) is colour-graded to illustrate carbonate-rich zone (the high MNF value is representative of limestone) with red colour. *b*, Position of image spectra collection point is plotted over grey scale MNF-1 image. *c*, Spectral profiles of surface exposures of limestone as delineated from MNF-1 image of three spectral map (1–6) are compared with ASTER SWIR band convolved laboratory spectra of limestone samples collected in the field.

the pixel. These differences are further averaged to calculate ‘noise’²⁹. In the second stage of MNF method, principal component of three input spectral maps is derived to form MNF-1 image keeping highest complementary information of three input maps. The MNF-1 image preserves the complementary information of different spectral maps and therefore is regarded as the composite spectral map after the image is histogram-equalized and colour-graded (to depict the high MNF value as representative of limestone) to show limestone exposures in red colour.

Discussion

In this study, we have demonstrated how different spectral maps can be used for mapping limestone, which is known for its diagnostic spectral feature within the SWIR domain. It is important to note that there are similarity in limestone distribution in these spectral maps (Figure 8 *a–c*), although with slight variation in the limestone distribution at few places. This is evident at the circular patch of open-cast mine, where limestone pixels are differently delineated as evident from each spectral map (Figure 8 *a–c*). Therefore, it was essential to integrate the commonalities of these spectral maps in an effective way, where correlative information of these spectral maps can be presented as a reliable limestone exposure map by removing non-coherent limestone pixels. In this regard, MNF method (as described earlier) is utilized efficiently to remove non-coherent limestone pixels of different spectral maps based on using ‘shift-difference method’ to derive a composite map.

Conclusion

Further, the composite map of limestone have been validated in light of existing geological and spectral data. This has been achieved by draping limestone boundary derived from a known geological map (modified after image interpretation and field survey) over a composite limestone map (Figure 9). Also, the SWIR band convolved image spectra of the limestone pixels of composite spectral map are collected from different parts of the image (Figure 10 *a* and *b*). These spectra are compared with the representative SWIR band convolved laboratory spectra of limestone (Figure 10 *c*). The observed similarity of these pixel spectra with laboratory spectra, justifies the composite limestone map derived using an integration of different spectral maps.

The approach of integration of spectral maps is essential to integrate the results of different spectral maps delineating the same target for demarcating it with better confidence, achieved by correlating the spectral maps. In the present study, MNF-based approach is used to derive a ‘composite’ limestone distribution map, which has a spatially coherent distribution of limestone pixels and the results are validated based on existing geological and spectral data. More importantly, the convergence attempted in the present study is reproducible in any other study where the convergence of the different spectral mapping algorithms are required for target mapping.

1. Bedini, E., Mineral mapping in the Kap Simpson complex, central East Greenland, using HyMap and ASTER remote sensing data. *Adv. Space Res.*, 2011, **47**, 60–73.
2. Brandmeier, M., Remote sensing of Carhuarazo volcanic complex using ASTER imagery in Southern Peru to detect alteration zones

- and volcanic structures – a combined approach of image processing in ENVI and ArcGIS/ArcScene. *Geocarto Int.*, 2010, **25**, 629–648.
3. Crosta, A. P., Filho, C. R. D. S., Azevedo, F. and Brodie, C., Targeting key alteration minerals in epithermal deposits in Patagonia, Argentina, using ASTER imagery and principal component analysis. *Int. J. Remote Sensing*, 2003, **24**, 4233–4240.
 4. Ditommaso, I. and Rubinstein, N., Hydrothermal alteration mapping using ASTER data in the Infiernillo porphyry deposit, Argentina. *Ore Geol. Rev.*, 2007, **32**, 275–290.
 5. Haselwimmer, C. E., Riley, T. R. and Liub, J. G., Lithologic mapping in the Oscar II Coast area, Graham Land, Antarctic Peninsula uses ASTER data. *Int. J. Remote Sensing*, 2011, **32**, 2013–2035.
 6. Zhang, X., Pazner, M. and Duke, N., Lithologic and mineral information extraction for gold exploration using ASTER data in the south Chocolate Mountains (California). *ISPRS J. Photogramm. Remote Sensing*, 2007, **62**, 271–282.
 7. Mars, J. C. and Rowan, L. C., Spectral assessment of new ASTER SWIR surface reflectance data products for spectroscopic mapping of rocks and minerals. *Remote Sensing Environ.*, 2010, **114**, 2011–2025.
 8. Kalinowski, A. and Oliver, S., *ASTER Mineral Index Processing Manual*; http://www.ga.gov.au/image_cache/GA7833.pdf 2004.
 9. Rowan, L. C. and Mars, J. C., Lithologic mapping in the Mountain Pass, California area using Advanced Spaceborne Thermal Emission and Reflection Radiometer (ASTER) data. *Remote Sensing Environ.*, 2003, **84**, 350–366.
 10. Sanjeevi, S., Targeting limestone and bauxite deposits in southern India by spectral unmixing of hyperspectral image data. *Int. Arch. Photogramm., Remote Sensing Spatial Inf. Sci.*, 2008, **XXXVII**, 1189–1194.
 11. Das, I. C., Aluminous laterite and bauxite ore deposits of Orissa, India identified by spectral signatures and spectral mixtures. *Indian Min. Eng. J. Mine TECH*, 2007, **7**, 62–67.
 12. Crowley, J. K., Visible and near-infrared spectra of carbonate rocks: reflectance variations related to petrographic texture and impurities. *J. Geophys. Res.*, 1986, **91**, 5001–2012.
 13. Gaffey, S. J., Spectral reflectance of carbonate minerals in the visible and near infrared (0.35–2.55 microns): calcite, aragonite, and dolomite. *Am. Mineral.*, 1986, **71**, 151–162.
 14. Valdiya, K. S., *The Making of India: Geodynamic Evolution*, Mcmillan India, 2010, 1st edn.
 15. Ghosh, S. K. and Chatterjee, B. K., Paleoenvironment reconstruction of early Proterozoic Kolhan siliciclastic rocks, Keonjhar districts, Orissa, India. *J. Geol. Soc. India*, 1990, **35**, 273–286.
 16. Mukhopadhyay, J., Ghosh, G., Nandi, Ajoy K., Chaudhuri and Asru, K., Depositional setting of the Kolhan Group: its implications for the development of a Meso to Neoproterozoic deep-water basin on the South Indian Craton. *S. Afr. J. Geol.*, 2006, **109**, 183–192.
 17. DGM, http://www.jharkhand.gov.in/new_depts/mines/geo/prospect.pdf (accessed on 3 January 2012)
 18. ASD Inc, 2012. Field spec specification; <http://www.asdi.com/products/fieldspecspectroradiometers/fieldspec-3-portable-spectroradiometer> (accessed on 3 September 2012).
 19. Guha, A. et al., Spectroscopic study of rocks of Hutti-Maski Schist Belt, Karnataka. *J. Geol. Soc. India*, 2012, **79**, 335–344.
 20. Guha, A., Rao, A., Ravi, S., Vinod Kumar, K. and Dhananjaya Rao, E. N., Analysis of the potential of kimberlite rock spectra as spectral end member using samples from Narayanpet kimberlite Field (NKF), Andhra Pradesh. *Curr. Sci.*, 2012, **103**(9), 1096–1104.
 21. Baldridge, A. M., Hook, S. J., Grove, C. I. and Rivera, G., The ASTER spectral library version 2.0. *Remote Sensing Environ.*, 2009, **113**, 711–715.
 22. Clark, R. N., Swayze, G. A., Heidebrecht, K., Green, R. O. and Goetz, A. F. H., Calibration to surface reflectance of terrestrial imaging spectrometry data: Comparison of methods. In *Summaries of the Fifth Annual JPL Airborne Geosciences Workshop*, Jet Propulsion Laboratory Special Publication, 1995, pp. 41–42.
 23. ENVI, *Atmospheric Correction Module: QUAC and FLAASH User's Guide*; <http://www.exelisvis.com/portals/0/pdfs/envi/FlaashModule.pdf2009>.
 24. Hubbard, B. E. and Crowley, J. K., Mineral mapping on the Chilean-Bolivian Altiplano using co-orbital ALI, ASTER and Hyperion imagery: data dimensionality issues and solutions. *Remote Sensing Environ.*, 2005, **99**, 173–186.
 25. Resmini, R. G., Kappus, M. E., Aldrich, W. S., Harsanyi, J. C. and Anderson, M., Mineral mapping with HYperspectral Digital Imagery Collection Experiment (HYDICE) sensor data at Cuprite, Nevada, USA. *Int. J. Remote Sensing*, 1997, **18**(7), 1553–1570.
 26. Rowan, L. C. and Mars, J. C., Lithologic mapping of the Mordor, NT, Australia ultramafic complex by using the Advanced Spaceborne Thermal Emission and Reflection Radiometer (ASTER). *Remote Sensing Environ.*, 2005, **99**, 105–126.
 27. van der Meer, F. D. and de Jong, S. M., *Imaging spectrometry: basic analytical techniques. In Imaging Spectrometry: Basic Principles and Prospective Applications*, Springer, Dordrecht, The Netherlands, 2001.
 28. Gabr, S., Ghulam, A. and Kusky, T., Detecting areas of high-potential gold mineralization using ASTER data. *Ore Geol. Rev.*, 2010, **38**, 59–69.
 29. Chen, X., Warner, T. A. and Campagna, D. J., Integrating visible, near-infrared and short-wave infrared hyperspectral and multi-spectral thermal imagery for geological mapping at Cuprite, Nevada. *Remote Sensing Environ.*, 2007, **110**, 344–356.
 30. Vitarello, I., Spectral discrimination of hydrothermally altered materials using ASTER short-wave infrared bands: evaluation in a tropical savannah environment. *Int. J. Appl. Earth Geoinf.*, 2005, **7**, 107–114.
 31. Farrand, W. and Harsanyi, J. C., Mapping the distribution of mine tailings in the Coeur d'Alene River Valley, Idaho, through the use of a constrained energy minimization technique. *Remote Sensing Environ.*, 1997, **59**, 64–76.
 32. Azizi, H., Tarverdi, M. and Akbarpour, A., Extraction of hydrothermal alterations of ASTER SWIR data from east Zanjan, northern Iran. *Adv. Space Res.*, 2010, **46**, 99–109.
 33. Bell, J. H., Bowen, B. B. and Martini, B. A., Imaging spectroscopy of jarosite cement in the Jurassic Navajo Sandstone. *Remote Sensing Environ.*, 2010, **114**, 2259–2270.
 34. Falcone, J. A. and Gomez, R., Mapping impervious surface type and sub-pixel abundance using Hyperion hyperspectral imagery. *Geocarto Int.*, 2005, **20**(4), 3–10.
 35. Roach, L. H., Mustard, J., Gendrin, A., Fernández-Remolar, D., Amils, R. and Amaral-Zettler, L., Finding mineralogically interesting targets for exploration from spatially coarse visible and near IR spectra. *Earth Planet. Sci. Lett.*, 2006, **252**, 201–214.

ACKNOWLEDGEMENTS. We thank the anonymous reviewer for constructive suggestions. We also thank the Directors, NRSC, Hyderabad and Jharkhand Space Application Centre, Ranchi for their support and encouragement; we also thank the Department of Geology and Mines, Government of Jharkhand for support during field work and also funding this project.

Received 20 June 2013; revised accepted 10 October 2013